Opto-Electronic Science

Original Article

2022, Vol. 1, No. 9

DOI: 10.29026/oes.2022.220004

100 Hertz frame-rate switching three-dimensional orbital angular momentum multiplexing holography via cross convolution

Weijia Meng[1,2], Yilin Hua[1,2]*, Ke Cheng[1,2], Baoli Li[1,2], Tingting Liu[1,2], Qinyu Chen[1,2], Haitao Luan[1,2], Min Gu[1,2]* and Xinyuan Fang[1,2]*

The orbital angular momentum (OAM) of light has been implemented as an information carrier in OAM holography. Holographic information can be multiplexed in theoretical unbounded OAM channels, promoting the applications of optically addressable dynamic display and high-security optical encryption. However, the frame-rate of the dynamic extraction of the information reconstruction process in OAM holography is physically determined by the switching speed of the incident OAM states, which is currently below 30 Hz limited by refreshing rate of the phase-modulation spatial light modulator (SLM). Here, based on a cross convolution with the spatial frequency of the OAM-multiplexing hologram, the spatial frequencies of an elaborately-designed amplitude distribution, namely amplitude decoding key, has been adopted for the extraction of three-dimensional holographic information encoded in a specific OAM information channel. We experimentally demonstrated a dynamic extraction frame rate of 100 Hz from an OAM multiplexing hologram with 10 information channels indicated by individual OAM values from –50 to 50. The new concept of cross convolution theorem can even provide the potential of parallel reproduction and distribution of information encoded in many OAM channels at various positions which boosts the capacity of information processing far beyond the traditional decoding methods. Thus, our results provide a holographic paradigm for high-speed 3D information processing, paving an unprecedented way to achieve the high-capacity short-range optical communication system.

Keywords: orbital-angular-momentum holography; multiplexing; high frame rate; switching; cross convolution

Meng WJ, Hua YL, Cheng K, Li BL, Liu TT et al. 100 Hertz frame-rate switching three-dimensional orbital angular momentum multiplexing holography via cross convolution. *Opto-Electron Sci* **1**, 220004 (2022).

Introduction

Holography provides a method to record and reconstruct both phase and amplitude of objects, which has achieved great success in various areas of data storage[1–4], three-dimensional display[5,6,7] and microcopy[8–10], etc. Various physical dimension, such as time[11], polarization[12–16], wavelength[17] and spatial or angle position[18,19], has been employed as independent information channels[20,21]. Such optically multiplexing holography supports high-capacity holographic information processing which can find applications in optical encryption[22], color display[23] and dynamic display[24]. Among these applications, information channels play significant roles. For instance, safety performance in encryption and

[1]Institute of Photonic Chips, University of Shanghai for Science and Technology, Shanghai 200093, China; [2]Centre for Artificial-Intelligence Nanophotonics, School of Optical-Electrical and Computer Engineering, University of Shanghai for Science and Technology, Shanghai 200093, China.

*Correspondence: YL Hua, E-mail: huayilin@usst.edu.cn; M Gu, E-mail: gumin@usst.edu.cn; XF Fang, E-mail: xinyuan.fang@usst.edu.cn

Received: 16 March 2022; Accepted: 9 June 2022; Published online: 7 September 2022

frame numbers in holographic display can be both improved by increasing the information channels. Abundant information channels in the holographic display could even support holographic video protocol.

To meet the ever-increasing demand for high-capacity optical devices in both classical and quantum information optics, the theoretical unbounded physical dimension of the orbital angular momentum (OAM)[25,26] has been used for optical multiplexing[27–30], optical communication[31,32] and quantum communication[33,34]. Recently, OAM has been implemented as an information carrier in holography, resulting in the concept of OAM holography. In OAM holography, the holographic information can only be reconstructed by the reconstructive beam with a specific helical phase distribution. Owing to the high-dimensional feature of the OAM, such OAM holography has attracted enormous interests in both linear holography[35,36] and nonlinear holography[37,38], even for the quantum OAM holography[39]. Notably, the information extraction rate from an OAM multiplexing hologram is a significant parameter, since the frame rate of a dynamic holographic display and the code rate of a holographic encryption system are both dominated by this parameter. Currently, the information extraction rate is mainly determined by the dynamic generation methods of the reconstructive beam with a specific OAM state.

Dynamically generating OAM carrying beams can be implemented based on various mechanisms: mechanical[40], thermal[41], optical[42,43] and electrical[44], etc. Traditional method for the information extraction is introducing an opposite phase term of $\exp(-il\varphi)$ to decode the information in a specific channel of a hologram with a spiral phase term of $\exp(il\varphi)$. Therefore, phase-modulation spatial light modulators (SLMs) are the most commonly used device to generate OAM carrying beams for information retrieval. However, the decoding rate is limited to below 30 Hz determined by the dynamic refresh rate of the device. In fact, this information extraction process leads to a convolution result between the vortex phase term of $\exp(-il\varphi)$ and the desired images in the spatial frequency domain[35,36]. Here, we develop a cross convolution theorem in the spatial frequency domain to achieve high-speed information extraction in OAM holography. We design an amplitude modulated pattern as a decoder, which is defined as an amplitude decoding key (ADK). In the spatial frequency domain, convolution between a series of spatial spectrum components of the ADK with the desired images takes place in our scheme to achieve the information extraction. As shown in Fig. 1, the OAM multiplexing Fourier transform hologram (FTH) is encoded with ten Arabic numerals ranging from 0 to 9 with different OAM charges ranging from –50 to 50, respectively. The different color refers to different information channel indicated by different OAM charge. Amplitude decoding keys are loaded on the digital micro-mirror device (DMD) to retrieve the information in these information channels. The lens near the DMD realizes a Fourier transform for the product of the hologram and the ADK, leading to a cross convolution between the spatial frequency of the OAM-multiplexing hologram and the spatial frequencies of the ADK

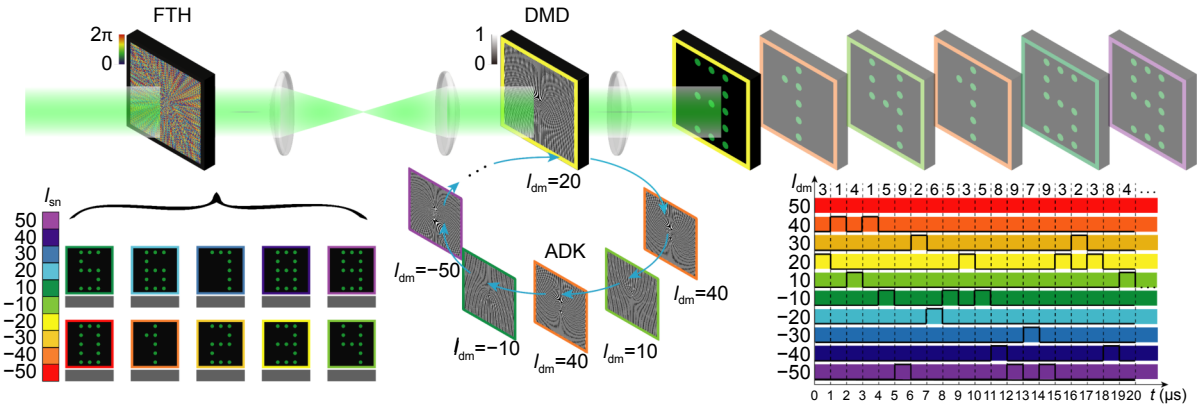

Fig. 1 | The schematical diagram of the high-frame-rate information extraction from an OAM multiplexing hologram. Ten images of the Arabic numerals ranging from 0 to 9 are encoded with OAM charges ranging from –50 to 50. Different colors represent different information channels indicated by specific OAM charges. Amplitude decoding keys are loaded on the DMD sequentially with corresponding decoding OAM charge for reproduction of the images. The lower right inset represents the time sequence for obtaining each image of the Arabic numeral by switching on the corresponding decoding patterns on DMD. Acquisition of the first few significant digits of the value π is illustrated in this figure.

and reproduce the image. By rapidly switching patterns (ADKs) according to the time sequence listed on the lower right inset (color represents the corresponding information channel similarly), the imaging plane will dynamically display a sequence of Arabic numerals. An information extraction frame rate of 100 Hz is demonstrated in our experiment for the transmission of the first 100 significant digits of the value π and the three-dimensional display of an image is verified based on this cross convolution theorem. In addition to the high information extraction speed, our scheme can further support the reproduction of an image in any desired position corresponding to a certain spatial spectrum component and parallel reproduction of images in different positions by employing multiple spatial spectrum components simultaneously, which greatly improves the flexibility and capacity of information processing in OAM holography.

Theoretical principle of the cross convolution theorem

The feasibility of rapid amplitude modulation provides the possibility to decode the information in each OAM channel with a high frame rate. Therefore, design of a specific amplitude distribution to serve as an ADK is the key component of this method. Decoding of an OAM selective hologram is first introduced to comprehend the physical principle of this method, as can be described in Fig. 2(a). Generation of an OAM selective hologram is illustrated on the inset map above the hologram in Fig. 2(a). The complex amplitude distribution of an OAM selective optical digital hologram can be described as:

$$H(x,y)=\sum_{u=1}^{M}\sum_{v=1}^{M}O(u,v)\exp\left[\mathrm{j}2\pi(ux+vy)\right]\cdot\exp\left(\mathrm{j}l_{\mathrm{sn}}\varphi_1\right), \tag{1}$$

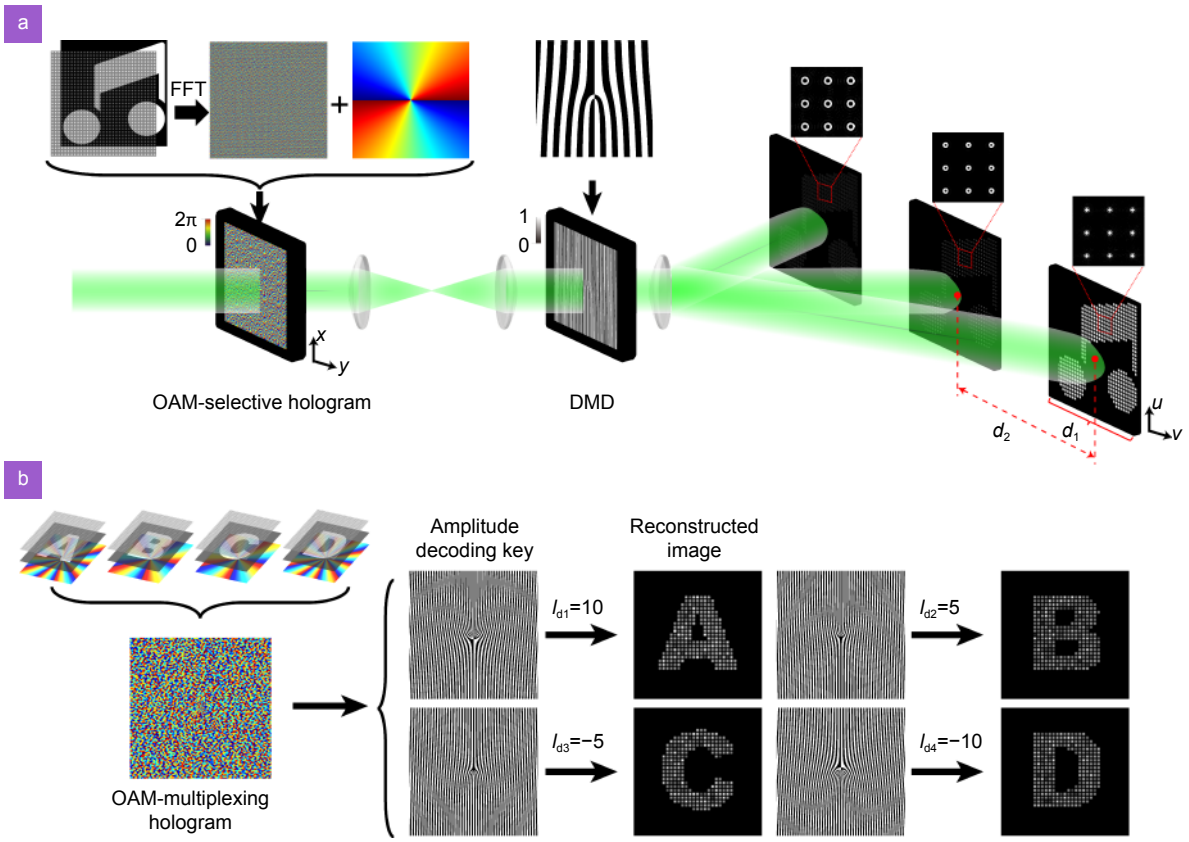

Fig. 2 | The schematic diagram of the information extraction from an OAM selective hologram and an OAM multiplexing hologram via cross convolution. (**a**) The principle of the cross convolution theorem for an OAM selective holography. For an OAM selective holography, the image (here, a music symbol) is sampled, Fourier transformed and superposed with a specific helical phase to form an OAM selective hologram. By applying corresponding ADK on the DMD, reproduction of the image can be displayed on the imaging plane. The ADK will result in a series of images due to its spatial frequency distribution. But only when the cross convolution theorem holds, these images are separated clearly and an exclusive image with basic Gaussian pixels will appear in a specific diffraction order. (**b**) The encoding and decoding process of OAM multiplexing holography. For OAM multiplexing holography, various images (four letters of an alphabet) are encoded in a single hologram with four OAM information channels indicated by OAM charge of –10, –5, 5 and 10. By applying the corresponding ADKs of these information channels, the images can be reconstructed.

here (x, y) and (u, v) represent the orthogonal coordinates in the hologram plane and the image plane and $O(u, v)$ is the target image. l_{sn} is the topological charge of the encoding OAM mode and φ_1 is the azimuth in the polar coordinates.

An ADK is loaded on the DMD to pertinently extract information in this hologram. The amplitude distribution pattern in the DMD can be considered as an interference of two beams of light, one of which is a vortex light carrying a topological charge number l_{dm}, and the other is an oblique plane wave, which has an angle θ with respect to the z-axis of the propagation direction. Since the DMD is a binary amplitude type device, its operation function can be expressed as:

$$a(\phi) = \begin{cases} 1, & \mathrm{mod}(\phi, 2\pi) \leqslant \pi \\ 0, & \text{others} \end{cases}, \tag{2}$$

where ϕ is the angular position in polar coordinates, depending on the interference result of $\phi = l_{dm}\varphi_1 - kx\sin\theta$[45], as displayed on the top inset of the DMD in Fig. 2(a). According to the Fourier series expansion, it can be rewritten in another form:

$$a(\phi) = \sum_{b=-\infty}^{+\infty} A_b \exp(\mathrm{i}b\phi), \tag{3}$$

here, b is the Fourier expansion order of the amplitude pattern and A_b is the Fourier expansion coefficient, which can be expressed as:

$$A_b = \frac{\sin(b\pi/2)}{b\pi}\exp\left(-\frac{\mathrm{i}b\pi}{2}\right). \tag{4}$$

This expansion results in a series of spatial frequency distributions in the following imaging plane where many diffraction orders appear.

When the incident light is a plane wave with finite aperture described by a circular aperture function (R stands for the radius), the light field at the near the rear surface of the DMD has a form of $circ(r_1/R)\cdot H(x, y)\cdot a(\phi)$, where $r_1 = \sqrt{x^2 + y^2}$ represents the radial coordinate on the plane of incident light. Therefore, the far field diffraction pattern at the imaging plane of the last lens is:

$$W(u, v) = c_1 \cdot \mathcal{F}\left[H(x, y)\cdot circ\left(\frac{r_1}{R}\right)\cdot a(\phi)\right], \tag{5}$$

where $c_1 = \exp(\mathrm{j}kf)\cdot\exp(\mathrm{j}ku^2/2f)\cdot\exp(\mathrm{j}kv^2/2f)/\mathrm{j}\lambda f$ represents a constant term irrelevant to the integral and $\mathcal{F}$ stands for Fourier transform operation. The Fourier transform of a product of $H(x, y)$ and $circ(r_1/R)\cdot a(\phi)$ can be expressed as a convolution between two spatial spectrums of these two terms, as can be described as:

$$W(u, v) = c_1 \cdot \mathcal{F}[H(x, y)] \otimes \mathcal{F}\left[circ\left(\frac{r_1}{R}\right)\cdot a(\phi)\right]. \tag{6}$$

For the simplicity of the calculation results, we define the product of $circ(r_1/R)$ and $\exp(\mathrm{i}l\varphi)$ as $V_{pp}|_l = circ(r_1/R)\exp(\mathrm{i}l\varphi)$, and its Fourier expression can be expressed as:

$$\mathcal{F}[V_{pp}|_l] = 2\pi(-\mathrm{j})^l\exp(\mathrm{i}l\varphi)\frac{R^2}{(l+2)\,l!}\left(\frac{kRr_2}{2f}\right)^l \cdot {}_1F_2\left[\frac{l+2}{2}, \frac{l+4}{2}, l+1; -\left(\frac{kRr_2}{2f}\right)^2\right], \tag{7}$$

where ${}_1F_2$ represents the confluent hypergeometric function[46,47]. The final far field distribution in the imaging plane can be calculated from the above expression with a form of:

$$W(u, v) = \sum_{b=-\infty}^{+\infty} A_b \cdot c_1 \cdot \sum_{u=1}^{M}\sum_{v=1}^{M} O\left(u + \frac{bk\sin\theta}{2\pi}, v\right) \otimes \mathcal{F}(V_{pp}|_{l_{sn}+bl_{dm}}). \tag{8}$$

Except for the constant part that will not affect the results, we can clearly see that the straightforward convolution result in Eq. (6) has been developed to a cross convolution[48] result, that is, the light field is composed of a cross convolution of the confluent hypergeometric function with the target image. This cross convolution result originates from the spatial frequency of the hologram and the spatial frequencies of the ADK, which are expanded as a series of diffraction orders according to Eq. (3).

From this result, two critical issues emerge as the key to the success of our protocol, which is defined as cross convolution theorem. The first issue is OAM sensitivity for the reproduction of the image. We can find that the appearance of the image is related both by the spatial frequency distribution (the diffraction orders displayed in the imaging plane) and the OAM charge of l_{dm}. The confluent hypergeometric function and the $\exp[\mathrm{i}(l_{sn} + bl_{dm})\varphi_2]$ term, commonly depend the reconstructed pixels feature, and the term of $O(u + bk\sin\theta/2\pi, v)$ depends displaced images which are introduced by spatial frequency distribution of the ADK according to the Eq. (8).

We can intuitively deduce the OAM selection rule of this protocol from Eq. (8) with a form of:

$$l_{sn} = -bl_{dm}. \tag{9}$$

It indicates that only the encoding OAM value and the

decoding OAM charge satisfy the above relationship can we obtain a clear image, in which each reconstructed pixel features the basic Gaussian mode dictated by a solid-spot intensity distribution, as can also be seen from the imaging results on Fig. 2(a). If the OAM selection rule is not satisfied, each pixel of the reconstructed image has an intensity distribution of doughnut type (as can be seen on the other diffraction orders of the imaging results in Fig. 2(a), the detailed discussion of the results with the mismatched decoding OAM charge can be found in Supplementary information). The energy distribution of the displaced images is determined by the Fourier expansion coefficient of the diffraction orders. For a high-quality holographic display, concentration of the most energy to a specific diffraction order should be implemented by the designing of the Fourier expansion coefficient of the ADK.

Since the image appears periodically in the imaging plane, the second issue is to prevent the overlap of these images. In the spatial frequency domain, d_2 represents the frequency spacing of the adjacent images, and d_1 represents the frequency bandwidth of the hologram, as can be found in Fig. 2(a). We can calculate that $d_1 = 1/p$ and $d_2 = k\sin\theta/2\pi$, where p represents the minimum pixel-cell size of the hologram. The minimum frequency spacing should exceed the frequency bandwidth of the hologram, so we can derive an equation $\sin\theta > \lambda/p$ that ensures the separability of those images from this minimum spatial frequency condition. The OAM selection rule and the minimum spatial frequency condition together constitute the two basic prerequisites of the cross convolution theorem, which lead to a clear image displayed in a specific location.

The cross convolution theorem can be naturally applied to an OAM multiplexing holography to extremely enhance the information extraction speed than the previous method. Multiple corresponding ADKs for each individual information channel are designed and switched to realize this function. As can be illustrated in Fig. 2(b), for each of the four letters, the OAM selective hologram was numerically engineered with different OAM charges of –10，–5，5，10, respectively, and then directly superimposed resulting in an OAM-multiplexing hologram (the details of generation of an OAM multiplexing hologram can be found in the Supplementary information). By dynamically switching four elaborately-designed ADKs with the decoding OAM charge of 10, 5, –5 and –10, one can successfully extract the information at the first diffraction order ($b = 1$), which satisfies the cross convolution theorem. The information acquisition speed can be as high as kilohertz with the switching speed of the ADKs by using the DMD.

Experimental results of three-dimensional and high-frame-rate OAM holography

The experimental setup for high-frame-rate information retrieval from an OAM selective hologram is illustrated in Fig. 3(a) according to the schematic diagram of Fig. 2(a). We start with a reproduction of the three-dimensional (3D) image of "IPC" (the abbreviation of the Institute of Photonic Chip) using the OAM selective holography. To implement a three-dimensional holographic display, several two-dimensional images that describe the shapes of the different cross sections of a 3D image must be projected to a series of planes and they should be all encoded in a single hologram. As demonstrated in the ref.[49], the Fourier transform hologram of these individual images of the letter "I", "P" and "C" are first per-shaped with a parabolic phase and then encoded with a same OAM charge ($l_s = 1$), which can ensure that the three images only reappear at each independent z_i coordinate clearly through Fresnel holography with the correct OAM selection rule. Therefore, the hologram has a form of:

$$H_n(x,y) = \sum_{n=1}^{3}\left\{\sum_{u=1}^{M}\sum_{v=1}^{M} O_n(u,v)\exp\left[\mathrm{j}2\pi(ux+vy)\right]\cdot\exp(\mathrm{j}l_s\varphi)\right\}\cdot\exp\left[-\mathrm{j}\frac{\pi}{\lambda z_n}(x^2+y^2)\right], \tag{10}$$

where $O_n(u,v)$ stands for three complex amplitude distributions of the three images and z_n is the position where the image is projected at. The hologram is loaded in the SLM and is illuminated by a CW-laser with a wavelength of 532 nm. The lens F_1, F_2 and pinhole before the SLM constitute the collimation and filtering system that filters the undesirable modes and provides a finite aperture of the light field. The ADK is loaded on the DMD with a decoding OAM charge of $l_{\mathrm{dm}} = -1$ and to match the most diffraction energy at $b = 1$. The SLM and the DMD are both reflective devices so that two beam splitters (BSs) combine these two devices to the main optical path. The lens F_3 and F_4 for a 4f system so that the hologram and the ADK meet the accurate imaging relationship. The last lens F_5 is a Fourier transform lens and the CCD is used to display the reconstructed image.

Different from the Fourier holography, Fresnel holography can operate at virtually any distance but the

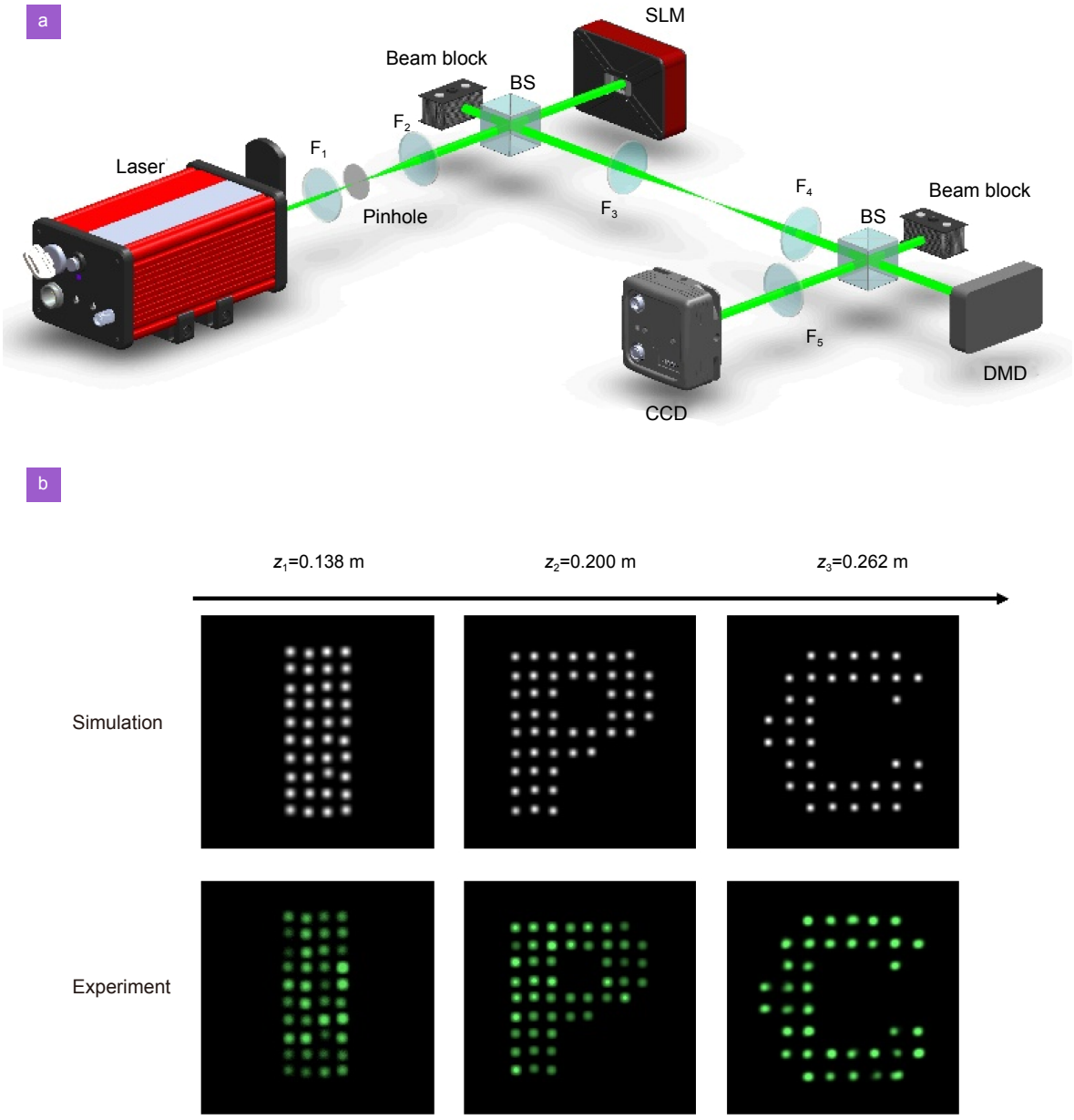

Fig. 3 | Three-dimensional holography based on the cross convolution theorem. (**a**) The experimental setup of three-dimensional holography with an OAM selective hologram via cross convolution. Three images of the letter "I", "P" and "C" with different *z* coordinates form a 3D image. They are first per-shaped with different parabolic phases and then encoded with a same OAM charge (l_s = 1) in an OAM selective hologram. The lens F_1, F_2 and pinhole before the SLM constitute the collimation and filtering system which provide a plane wave illumination of the hologram with a finite aperture. The SLM and DMD are loaded with OAM selective hologram and corresponding ADK, respectively. They are coupled to the main optical path through two beam splitters and they meet the accurate imaging relationship through the two lenses of F_3 and F_4. CCD is moved to obtain the reconstructed images of the letters through the imaging lens of F_5. (**b**) The simulation and experimental results of this holographic 3D display based on cross convolution theorem.

wavefront of this type of hologram will become locally flat at a specific distance determined by the parabolic phase encoded. It can be described as following:

$$W(u,v,z_i) = c_2 \cdot \mathcal{F}\left\{H_n(x,y) \cdot circ\left(\frac{r_1}{R}\right) \cdot a(\phi) \cdot \exp\left[\mathrm{j}\frac{\pi}{\lambda z_i}(x^2+y^2)\right]\right\}. \quad (11)$$

where z_i is any distance between arbitrary imaging plane with the lens F_5 and $c_2 = \exp(\mathrm{j}kz_i) \cdot \exp(\mathrm{j}ku^2/2z_i) \cdot \exp(\mathrm{j}kv^2/2z_i)/\mathrm{j}\lambda z_i$ represents a constant term. We can find that only when $z_i = z_n$, the parabolic phase can be compensated and we can obtain a similar result as that of the theoretical model. A huge noisy term appears on the image in other positions which makes the image drawn

in the noise[49]. Therefore, by scanning the CCD in a specific position and following the cross convolution theorem, the three letters will appear in three positions with the z coordinates of 0.138 m, 0.2 m and 0.262 m, respectively. The experimental results are completely consistent with the simulation results which can be found in Fig. 3(a) and Fig. 3(b), leading to a holographic display of a 3D image. In fact, our scheme can be extended to the realization of the reproduction of a more complex 3D object with continuous z profiles by combining plenty of two-dimensional images in an OAM selective hologram. However, the crosstalk between the reconstructed images may reduce the imaging quality (the details of the discussion on the realization of OAM holography of a real 3D object can be found in Supplementary information).

Due to the high-frame-rate switching feature of the ADKs, a high-speed information retrieval from an OAM multiplexing hologram can be implemented. We take the rapid retrieval of the first 100 significant digits of the π as an example, which represents a fast information transfer network can be established with OAM multiplexing holography. Figure 4(a) is the OAM multiplexing FTHs which encode 10 types of Arabic numerals ranging from 0 to 9 with different OAM charges ranging from –50 to 50. Choosing the OAM spacing of 10 to encode each image of Arabic numeral can ensure the negligible crosstalk and increase the signal to noise ratio for information reproduction (see the detailed discussion of the OAM spacing chosen in the Supplementary information). The CCD is fixed at the focal plane of the lens F_5 so this is a standard Fourier holography. All of the ADKs are designed to concentrate the most energy on their first order. Therefore, by following the cross convolution theorem and switching the corresponding ADKs with the opposite decoding OAM charge ($l_{dm} = -l_{sn}$, $b = 1$) with correct time sequence (as illustrated in lower right inset of Fig. 1), the first 100 significant digits of the π appear at

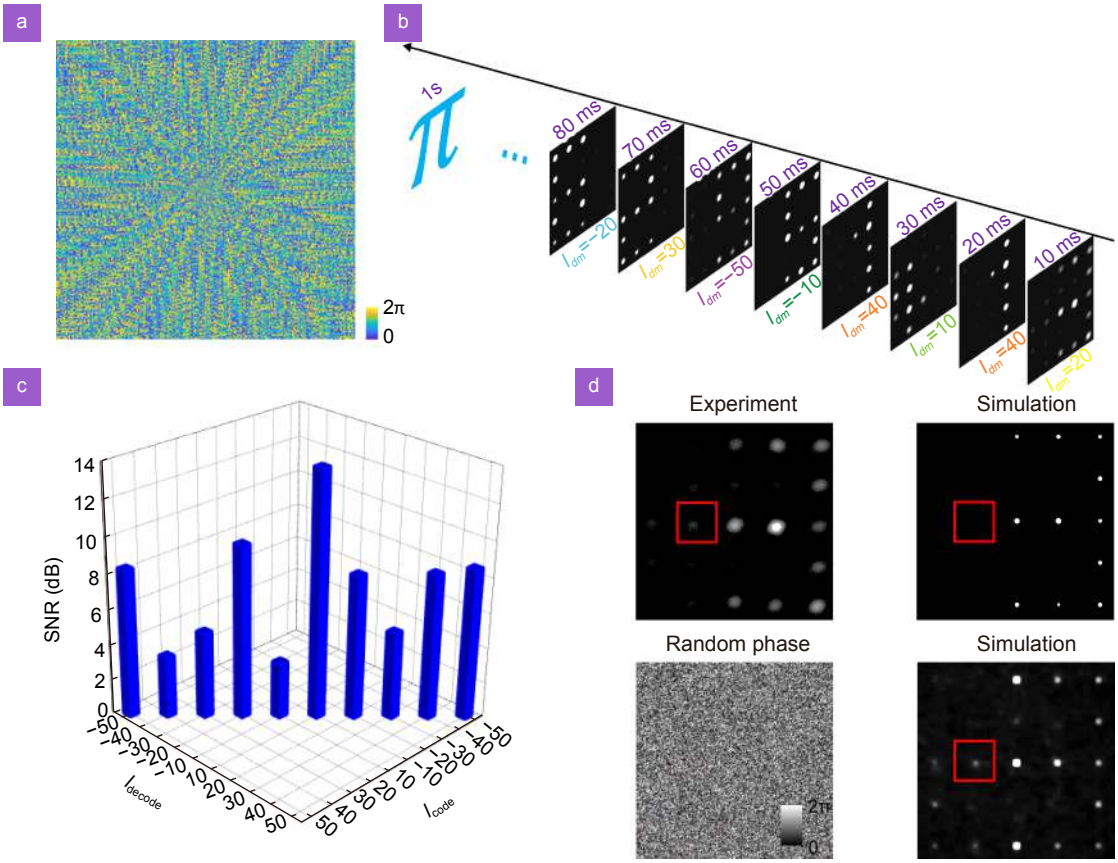

Fig. 4 | A high-frame-rate information transmission example through OAM multiplexing holography based on cross convolution theorem. (**a**) The OAM multiplexing hologram which contains ten images of the Arabic numerals ranging from 0 to 9 encoded with OAM charges ranging from –50 to 50. (**b**) Sequential transmission of the first 100 significant digits of the value π through holography. (**c**) The individual SNRs for each image of the Arabic numeral. (**d**) The simulation and experimental results of holographic reconstruction of a specific image of an Arabic numeral "3".

the CCD sequentially. The experimental result of obtaining the first a few significant digits of π is displayed in Fig. 4(b). The switching rate is set to 100 Hz so that the 100 significant digits can be transferred in a duration of one second. Current switching rate in our experiment is mainly restricted by the refresh rate of the CCD rather than the switching speed of the ADKs. By applying the ultra-high-speed camera as the display device, the information retrieval frame rate can be enhanced to kilohertz. Compared to the maximum decoding rate of below 30 Hz in OAM multiplexing holography[35] which was limited by the phase modulated SLM, two orders of magnitude enhancing in decoding rate can be realized using our protocol.

Fig. 4(c) indicates the signal to noise ratio (SNR) for each Arabic numeral during the transmission. We can see that although different information channel has different SNR in holography, identification of all these Arabic numerals is still possible in our experiments. Fig. 4(d) displays a specific numeral "3" we obtained in the experiment. We can find that an undesirable pixel appears in the experimental result, while it is absent in the simulation. This point is caused by the random phase added on the FTH or the phase noise generated in the optical path in practical experimental process. For example, the phase linearity matching error of the SLM or the unevenness of the SLM liquid crystal reflective surface could both introduce this random phase added on the FTH. It is proved by the simulation result when considering the random phase added on the FTH, since it has similar results as that of the experiment. By compensating the unwanted phase noise caused either by the SLM or the devices used in the optical path could eliminate the effect and improve the imaging quality.

Discussion

A fascinating phenomenon of our protocol is that OAM selection rule in cross convolution theorem is $l_{sn} = -bl_{dm}$, leading to the appearance of the image emerging periodically in the spatial frequency domain. But only the correct value of b and l_{dm} can ensure a perfect image composed of basic Gaussian pixels, so that optimization of the spatial frequency distribution of the ADK can improve the imaging efficiency in holography. Thus, the energy can be concentrated on this correct spatial frequency position. On the other hand, by adjusting the spatial frequency distribution such that each spatial frequency position occupies a considerable energy, reproduction of the images can be simultaneously implemented at different positions as long as the product of bl_{dm} is equal to the encoding OAM charge of l_{sn}. For one switch that l_{dm} is fixed, different b stands for different information terminal to receive information encoded in different OAM channels with corresponding l_{sn}. For a hologram with plenty of information channels, switching the ADKs can even lead to the presentation of the refreshed information at different terminals. It provides a possibility to parallelly extract and distribute information encoded in many OAM channels to multiple locations at one time with light in a short range, just like the scenery described by the wireless communication system, so called Lifi[50]. In this way, our protocol based on the cross convolution theorem can boost the capacity for information processing which has the potential to be extended to other applications such as construction of a high-capacity short-range optical communication system. The cross convolution protocol has better to be slightly adjusted in this case by replacing the amplitude decoding key to a similar phase decoding key which contains the same spatial spectrums, i.e., employing a second SLM to carry this phase decoding key. The advantage of this operation is a huge improvement in diffraction efficiency[51,52] of different spatial spectra which is beneficial to clear display of multiple images simultaneously, although the refresh rate is reduced to tens of Hertz.

It is worth mentioning that some advanced technologies such as meta-holography[53,54] and high-speed imaging will further improve the performance of our protocol. For example, through involving a metasurface for recoding OAM multiplexing hologram, a more frame number of images can be encoded and the spatial bandwidth product of the transmitted images could be greatly enhanced owing to its subwavelength resolution[55,56], given that encoded OAM range increases directly with the improvement of the resolution (see the detailed discussion in the Supplementary information). Moreover, the frame-rate of the information extraction in our system is currently limited by the frame-rate of the camera. However, the recent progress in high-speed imaging using various high-performance cameras has exceeded a frame rate of kilohertz[57,58] which could match the switching frame-rate of the ADKs.

Conclusions

In summary, a high-frame-rate dynamic extraction of the information encoded in the OAM multiplexing

hologram is demonstrated using a novel protocol of cross convolution. Based on the cross convolution theorem, an experimental reproduction of a 3D image is verified using the OAM selective holography, and the information transfer of the first 100 significant digits of π is demonstrated with a frame-rate of 100 Hz using OAM multiplexing holography. Current OAM multiplexing holography based on cross convolution theorem has huge potential to further improve the information retrieval frame-rate by introducing high-speed imaging system. Combination of the advantage of high-speed imaging system and high frame-number meta-holography technology with our protocol will lead to a high-speed transmission of massive information using OAM holography, which can find applications ranging from dynamic display to short-range optical communication.

References

1. Yoneda N, Saita Y, Nomura T. Computer-generated-hologram-based holographic data storage using common-path off-axis digital holography. *Opt Lett* **45**, 2796–2799 (2020).
2. Hesselink L, Orlov SS, Bashaw MC. Holographic data storage systems. *Proc IEEE* **92**, 1231–1280 (2004).
3. Buse K, Adibi A, Psaltis D. Non-volatile holographic storage in doubly doped lithium niobate crystals. *Nature* **393**, 665–668 (1998).
4. Lin X, Liu J P, Hao JY, Wang K, Zhang YY et al. Collinear holographic data storage technologies. *Opto-Electron Adv* **3**, 190004 (2020).
5. Geng J. Three-dimensional display technologies. *Adv Opt Photonics* **5**, 456–535 (2013).
6. Shi L, Li BC, Kim C, Kellnhofer P, Matusik W. Towards real-time photorealistic 3D holography with deep neural networks. *Nature* **591**, 234–239 (2021).
7. Gao H, Fan XH, Xiong W, Hong MH. Recent advances in optical dynamic meta-holography. *Opto-Electron Adv* **4**, 210030 (2021).
8. Singh V, Tayal S, Mehta DS. Highly stable wide-field common path digital holographic microscope based on a Fresnel biprism interferometer. *OSA Continuum* **1**, 48–55 (2018).
9. Faridian A, Pedrini G, Osten W. Opposed-view dark-field digital holographic microscopy. *Biomed Opt Express* **5**, 728–736 (2014).
10. Zheng JJ, Gao P, Shao XP. Opposite-view digital holographic microscopy with autofocusing capability. *Sci Rep* **7**, 4255 (2017).
11. Li JX, Kamin S, Zheng GX, Neubrech F, Zhang S et al. Addressable metasurfaces for dynamic holography and optical information encryption. *Sci Adv* **4**, eaar676 (2018).
12. Mueller JPB, Rubin NA, Devlin RC, Groever B, Capasso F. Metasurface polarization optics: independent phase control of arbitrary orthogonal states of polarization. *Phys Rev Lett* **118**, 113901 (2017).
13. Wu RY, Zhao YQ, Li N, Kong SG. Polarization image demosaicking using polarization channel difference prior. *Opt Express* **29**, 22066–22079 (2021).
14. Hong YQ, Han SK. Polarization-dependent SOA-based PolSK modulation for turbulence-robust FSO communication. *Opt Express* **29**, 15587–15594 (2021).
15. Duan YH, Zhang F, Pu MB, Guo YH, Xie T et al. Polarization-dependent spatial channel multiplexing dynamic hologram in the visible band. *Opt Express* **29**, 18351–18361 (2021).
16. Wang JY, Tan XD, Qi PL, Wu CH, Huang L et al. Linear polarization holography. *Opto-Electron Sci* **1**, 210009 (2022).
17. Li X, Chen LW, Li Y, Zhang XH, Pu MB et al. Multicolor 3D meta-holography by broadband plasmonic modulation. *Sci Adv* **2**, e1601102 (2016).
18. Kamali SM, Arbabi E, Arbabi A, Horie Y, Faraji-Dana M et al. Angle-multiplexed metasurfaces: encoding independent wavefronts in a single metasurface under different illumination angles. *Phys Rev X* **7**, 041056 (2017).
19. Gao H, Wang YX, Fan XH, Jiao BZ, Li TA et al. Dynamic 3D meta-holography in visible range with large frame number and high frame rate. *Sci Adv* **6**, eaba8595 (2020).
20. Fang XY, Ren HR, Li KY, Luan HT, Hua YL et al. Nanophotonic manipulation of optical angular momentum for high-dimensional information optics. *Adv Opt Photonics* **13**, 772–833 (2021).
21. Gu M, Fang XY, Ren HR, Goi E. Optically digitalized holography: a perspective for all-optical machine learning. *Engineering* **5**, 363–365 (2019).
22. Georgi P, Wei QS, Sain B, Schlickriede C, Wang YT et al. Optical secret sharing with cascaded metasurface holography. *Sci Adv* **7**, eabf9718 (2021).
23. Bao YJ, Yu Y, Xu HF, Guo C, Li JT et al. Full-colour nanoprint-hologram synchronous metasurface with arbitrary hue-saturation-brightness control. *Light Sci Appl* **8**, 95 (2019).
24. Wu ZG, Zhou XW, Wu SY, Yan ZK, Li Y et al. Dynamic holographic display based on perovskite nanocrystal doped liquid crystal film. *IEEE Photonics J* **13**, 6 (2021).
25. Fang XY, Kuang ZY, Chen P, Yang HC, Li Q et al. Examining second-harmonic generation of high-order Laguerre-Gaussian modes through a single cylindrical lens. *Opt Lett* **42**, 4387–4390 (2017).
26. Wei D, Guo JL, Fang XY, Wei DZ, Ni R et al. Multiple generations of high-order orbital angular momentum modes through cascaded third-harmonic generation in a 2D nonlinear photonic crystal. *Opt Express* **25**, 11556–11563 (2017).
27. Tang RK, Li XJ, Wu WJ, Pan HF, Zeng HP et al. High efficiency frequency upconversion of photons carrying orbital angular momentum for a quantum information interface. *Opt Express* **23**, 9796–9802 (2015).
28. Gruneisen MT, Miller WA, Dymale RC, Sweiti AM. Holographic generation of complex fields with spatial light modulators: application to quantum key distribution. *Appl Optics* **47**, A32–A42 (2008).
29. Gong L, Zhao Q, Zhang H, Hu XY, Huang K et al. Optical orbital-angular-momentum-multiplexed data transmission under high scattering. *Light Sci Appl* **8**, 27 (2019).
30. Zhu L, Wang J. A review of multiple optical vortices generation: methods and applications. *Front Optoelectron* **12**, 52–68 (2019).
31. Willner AE, Huang H, Yan Y, Ren Y, Ahmed N et al. Optical communications using orbital angular momentum beams. *Adv Opt Photonics* **7**, 66–106 (2015).
32. Wang J, Chen S, Liu J. Orbital angular momentum communications based on standard multi-mode fiber (invited paper). *APL*

Photonics **6**, 060804 (2021).
33. Liu J, Nape I, Wang Q, Vallés A, Wang J et al. Multidimensional entanglement transport through single-mode fiber. *Sci Adv* **6**, eaay0837 (2020).
34. Wang QK, Wang FX, Liu J, Chen W, Han ZF et al. High-dimensional quantum cryptography with hybrid orbital-angular-momentum states through 25 km of ring-core fiber: a proof-of-concept demonstration. *Phys Rev Appl* **15**, 064034 (2021).
35. Ren HR, Fang XY, Jang J, Bürger J, Rho J et al. Complex-amplitude metasurface-based orbital angular momentum holography in momentum space. *Nat Nanotechnol* **15**, 948–955 (2020).
36. Fang XY, Ren HR, Gu M. Orbital angular momentum holography for high-security encryption. *Nat Photonics* **14**, 102–108 (2020).
37. Fang XY, Yang HC, Yao WZ, Wang TX, Zhang Y et al. High-dimensional orbital angular momentum multiplexing nonlinear holography. *Adv Photonics* **3**, 015001 (2021).
38. Fang XY, Wang HJ, Yang HC, Ye ZL, Wang YM et al. Multichannel nonlinear holography in a two-dimensional nonlinear photonic crystal. *Phys Rev A* **102**, 043506 (2020).
39. Kong LJ, Zhang FR, Zhang JF, Sun YF, Zhang XD. High-dimensional entanglement-enabled holography for quantum encryption. (2021); http://doi.org/10.21203/rs.3.rs-658825/v1.
40. Cai XL, Wang JW, Strain MJ, Johnson-Morris B, Zhu JB et al. Integrated compact optical vortex beam emitters. *Science* **338**, 363–366 (2012).
41. Al-Attili AZ, Burt D, Li Z, Higashitarumizu N, Gardes FY et al. Germanium vertically light-emitting micro-gears generating orbital angular momentum. *Opt Express* **26**, 34675–34688 (2018).
42. Cao FL, Zhao Y, Yao CH, Xie CQ. All diffractive optical element setup for creating and characterizing optical vortices with high topological charges: analytical models and numerical results. *Opt Commun* **495**, 127119 (2021).
43. Li K, Tang KF, Lin D, Wang J, Li BX et al. Direct generation of optical vortex beams with tunable topological charges up to 18th using an axicon. *Opt Laser Technol* **143**, 107339 (2021).
44. Wang Y, Zhao P, Feng X, Xu YT, Cui KY et al. Integrated photonic emitter with a wide switching range of orbital angular momentum modes. *Sci Rep* **6**, 22512 (2016).
45. Carpentier AV, Michinel H, Salgueiro JR, Olivieri D. Making optical vortices with computer-generated holograms. *Am J Phys* **76**, 916–921 (2008).
46. Gradshteyn IS, Ryzhik IM. *Table of Integrals*, *Series*, *and Products* 8th ed (Academic Press, Cambridge, 2014).
47. Prudnikov AP, Brychkov YA, Marichev OI. *Integrals and Series Vol 2: Special Functions* (Gordon and Breach, New York, 1986).
48. Qiu XD, Li FS, Liu HG, Chen XF, Chen LX. Optical vortex copier and regenerator in the Fourier domain. *Photonics Res* **6**, 641–646 (2018).
49. Makey G, Yavuz Ö, Kesim DK, Turnalı A, Elahi P et al. Breaking crosstalk limits to dynamic holography using orthogonality of high-dimensional random vectors. *Nat Photonics* **13**, 251–256 (2019).
50. Shan QS, Wei CT, Jiang Y, Song JZ, Zou YS et al. Perovskite light-emitting/detecting bifunctional fibres for wearable LiFi communication. *Light Sci Appl* **9**, 163 (2020).
51. Ketchum RS, Blanche PA. Diffraction efficiency characteristics for MEMS-based phase-only spatial light modulator with nonlinear phase distribution. *Photonics* **8**, 62 (2021).
52. Turtaev S, Leite IT, Mitchell KJ, Padgett MJ, Phillips DB et al. Comparison of nematic liquid-crystal and DMD based spatial light modulation in complex photonics. *Opt Express* **25**, 29874–29884 (2017).
53. Kim I, Jang J, Kim G, Lee J, Badloe T et al. Pixelated bifunctional metasurface-driven dynamic vectorial holographic color prints for photonic security platform. *Nat Commun* **12**, 3614 (2021).
54. Wang DY, Liu FF, Liu T, Sun SL, He Q et al. Efficient generation of complex vectorial optical fields with metasurfaces. *Light Sci Appl* **10**, 67 (2021).
55. Meng Y, Chen YZ, Lu LH, Ding YM, Cusano A et al. Optical meta-waveguides for integrated photonics and beyond. *Light Sci Appl* **10**, 235 (2021).
56. Tseng E, Colburn S, Whitehead J, Huang LC, Baek SH et al. Neural nano-optics for high-quality thin lens imaging. *Nat Commun* **12**, 6493 (2021).
57. Matin A, Wang X. Compressive coded rotating mirror camera for high-speed imaging. *Photonics* **8**, 34 (2021).
58. https://www.gaosuxiangji.com/products/detail/nid/3747.html.

Acknowledgements

We would like to acknowledge the support from the Science and Technology Commission of Shanghai Municipality (Grant No. 21DZ1100500), the Shanghai Municipal Science and Technology Major Project, the Shanghai Frontiers Science Center Program (2021-2025 No. 20),the Zhangjiang National Innovation Demonstration Zone (Grant No. ZJ2019-ZD-005), the Shanghai Rising-Star Program (20QA1404100) and National Natural Science Foundation of China (62005164, 62005166, 12004355).

Author contributions

X. Y. Fang proposed the original idea. M. Gu and X. Y. Fang supervised the project. W. J Meng and Y. L. Hua completed the theoretical model and performed the experiments. All the authors contributed to the the analysis of the experiment result and the paper writing.

Competing interests

The authors declare no competing financial interests.

Supplementary information

Supplementary information for this paper is available at https://doi.org/10.29026/oes.2022.220004